



Cloud albedo changes in response to anthropogenic sulfate and non-sulfate aerosol forcings in CMIP5 models

Lena Frey¹, Frida A.-M. Bender¹, and Gunilla Svensson¹

¹Department of Meteorology and Bolin Centre for Climate Research, Stockholm University, Stockholm, Sweden

Correspondence to: Lena Frey (lena.frey@misu.su.se)

Abstract. The effects of different aerosol types on cloud albedo are analyzed using the linear relation between total albedo and cloud fraction found on monthly mean scale in regions of subtropical marine stratocumulus clouds, and the influence of Aerosol Optical Depth (AOD) on this relation. Model experiments from the Coupled Model Intercomparison Project phase 5 (CMIP5) are used to separately study the responses to increases in sulfate, non-sulfate and all anthropogenic aerosols. A cloud brightening on month-to-month scale due to variability in the background aerosol is found to dominate even in the cases where anthropogenic aerosols are added. The aerosol composition is found to be of importance for this cloud brightening, that is thereby region dependent. There is indication that absorbing aerosols to some extent counteract the cloud brightening, but scene darkening with increasing aerosol burden is generally not supported, even in regions where absorbing aerosols dominate. Regional, monthly mean cloud albedo is found to increase with the addition of anthropogenic aerosols, and more so with sulfate than non-sulfate. The changes in AOD due to anthropogenic aerosols are typically small compared to the AOD variability within a given aerosol forcing scenario, and the magnitude of the change in cloud albedo due to anthropogenic aerosols is small and not directly related to the strength of the month-to-month cloud brightening due to aerosols. The diversity in changes in cloud albedo in this set of models is rather related to the different changes in cloud water content between the experiments.

1 Introduction

Aerosol particles have an impact on the radiation budget of the Earth, directly through interaction with radiation and indirectly via interaction with clouds. Taking into account the counteracting effects of scattering and absorbing aerosols, the net forcing from all aerosols, including their interactions with clouds, is estimated to be negative, implying a cooling of the climate. The magnitude of the cooling remains uncertain (Boucher et al., 2013) and although smaller forcings and narrower uncertainty ranges have been suggested (Stevens, 2015), the most recent report from the Intergovernmental Panel on Climate Change (IPCC) estimates the effective radiative forcing due to aerosols, including cloud adjustments, to -0.9 Wm^{-2} , with a 90% uncertainty range of -1.9 to -0.1 Wm^{-2} . Hereby, aerosols contribute the largest uncertainty to the total radiative forcing estimate from pre-industrial time (Myhre et al., 2013b).

One factor contributing to this uncertainty is the dependence of aerosol-cloud interactions on aerosol type. Aerosols can serve as cloud condensation nuclei (CCN) dependent on their chemical and physical properties, like hygroscopicity and size, and be



activated to form cloud droplets. Assuming a constant liquid water path (LWP), a cloud with a larger number of available CCN will have more numerous and smaller cloud droplets, and therefore a higher cloud albedo. This cloud brightening effect due to aerosols is known as the cloud albedo or Twomey effect (Twomey, 1977). Smaller cloud droplets can also increase the lifetime of a cloud by reducing the precipitation efficiency as described by the cloud lifetime or Albrecht effect (Albrecht, 1989).
5 Absorbing aerosols that are less efficient as CCN may instead reduce cloud cover, as suggested by e.g. Ackerman et al. (2000). These, and the many additional possible pathways for aerosol influence on cloud properties, are difficult to disentangle, but the strength of the individual effects and their net effect are dependent on the properties of the underlying aerosol distribution.

In this study we separate the effects of sulfate and non-sulfate aerosols on cloud albedo. We focus on marine subtropical stratocumulus clouds, that have been found to be highly sensitive to aerosol perturbations (Wood, 2012), and coincide with
10 regions of maximum forcing from the cloud albedo effect (Carslaw et al., 2013). Stratocumulus clouds cover more than 20% of the Earth's surface (Wood, 2012), and low clouds play a major role for the radiation budget of the Earth (Slingo, 1990; Hartmann et al., 1992), particularly in marine subtropical regions, due to their reflection of shortwave solar radiation in regions with high insolation and dark underlying surface. In addition, marine stratocumulus clouds are the main source of uncertainty concerning tropical cloud feedbacks (Bony and Dufresne, 2005), and their representation in climate models has been pointed
15 out as problematic (Bender et al., 2006; Karlsson et al., 2008). A specific issue is the compensation between amount and brightness in low altitude and low latitude clouds, referred to as the "too few, too bright" problem, described by Nam et al. (2012), leading to an overestimation of the cloud albedo especially in tropical and subtropical regions (Karlsson et al., 2008; Myhre et al., 2013a).

A method for quantifying cloud albedo on monthly mean regional scale in climate models and satellite observations was
20 introduced by Bender et al. (2011). Hereby, the cloud albedo was determined based on the linear relation between cloud fraction and albedo found in five regions of low-altitude subtropical marine stratocumulus clouds, defined in Klein and Hartmann (1993). By separation of the clear sky albedo α_{clear} and the cloud albedo α_{cloud} , the total albedo α can be defined as,

$$\alpha = \alpha_{cloud} \cdot f_c + \alpha_{clear} \cdot (1 - f_c) \quad (1)$$

with the cloud fraction f_c . The linear relation between albedo and cloud fraction indicates a constant cloud albedo, which
25 can thus be estimated as the sum of slope and intercept found from a linear regression of α onto f_c . A comparison between preindustrial and present-day simulations shows a cloud albedo increase due to changed anthropogenic aerosol emissions (Engström et al., 2014), using this method.

With the aim to address how aerosol variations affect the cloud albedo in a given aerosol emission scenario, an approach to relate the Aerosol Optical Depth (AOD) to the cloud albedo was introduced by Bender et al. (2016). The AOD is a measure of
30 the amount of solar radiation which is reflected and absorbed by aerosols and is well correlated with the number concentration of CCN over large spatial scales (Andreae, 2009). The impact of aerosols on cloud albedo was investigated by analysing the distribution of AOD anomaly in the albedo-cloud fraction space, assuming that an increase in aerosol emissions would cause an increase both in AOD and in number of available CCN, that may in turn increase the number of cloud droplets and the cloud albedo. Model results of present-day simulations showed a cloud brightening related to aerosols in all the subtropical



stratocumulus regions studied, whereas no effect or in some regions a reversed relation was found for satellite data (Bender et al., 2016). It was suggested that counteracting scene darkening could be caused by absorbing aerosols overlying the cloud and that this is not well represented in the models.

In this study we investigate further how different aerosol types affect the cloud albedo in climate models. We use model output of sensitivity experiments from the Coupled Model Intercomparison Project phase 5 (CMIP5, Taylor et al. (2012)) with separated aerosol forcings to analyze the effect of all anthropogenic aerosols as well as sulfate and non-sulfate aerosols, respectively. We analyze the AOD anomaly in the albedo-cloud fraction space and study the spread around the approximately linear relation to determine the influence of aerosol on albedo for a given cloud fraction, for each forcing scenario. We refer to this as "cloud brightening on month-to-month scale" and the results of this analysis are presented in Sect. 3.3. In the same section we also compare estimated cloud albedo changes between the different forcing scenarios, i.e. cloud brightening due to changed aerosol forcing, and investigate the relation between the two, and other potential factors determining the magnitude of the cloud albedo change. In addition, we study the representation of aerosols in the different CMIP5 models, further examining the large variation in AOD found on the global mean scale among climate models (Shindell et al., 2013) (Sect. 3.2). In Sect. 2 we describe the model output and analysis method and we discuss and summarize our findings in Sect. 4.

2 Model output and data processing

To analyze the effects of separated aerosol types on the cloud albedo, we use model output from three experiments (*sstClim*, *sstClimAerosol* and *sstClimSulfate* according to the CMIP5 protocol) with different aerosol emissions. For all experiments, the models were run in AMIP-type configuration with a fixed SST and sea ice climatology. In the reference simulation, the aerosol emissions were kept on a preindustrial level corresponding to the year 1850. We refer to this simulation as the 'Control' experiment. For the sensitivity experiments, all forcings were kept on a preindustrial level except the aerosol forcing, so that changes in the cloud albedo are assumed to be caused only by aerosol concentration changes. For the first sensitivity experiment, referred to as the 'All Aerosol' experiment, the emissions of all anthropogenic aerosol types were set to the level of year 2000 from the corresponding historical simulation. In the second sensitivity experiment, referred to as 'Sulfate Only', only the emissions of sulfate aerosols were set to the level of year 2000. The effects of non-sulfate aerosols are derived by calculating the difference between the All Aerosol and Sulfate Only simulations, cf. Zelinka et al. (2014). Adding this residual deviation to the control simulation gives the influence from non-sulfate aerosols, which we refer to as the 'Non Sulfate' case. A complementing experiment with only black carbon (BC) aerosol emissions set to the level of year 2000, will be discussed briefly as it was only performed with one model (NorESM). This experiment is referred to as 'BC Only'. With this simulation the influence of BC and other non-sulfate aerosols can be separated.

Aerosol particles which are parameterized in the studied models are dust, sea salt, sulfate, BC and organic matter (OM), where OM includes primary and secondary organic aerosol except for HadGEM (secondary only). All aerosol types on the preindustrial level are present in all experiments, and only anthropogenic aerosol emissions are altered in the sensitivity experiments. This means that the non-sulfate aerosol difference is assumed to be attributable to BC and OM, since these are the



non-sulfate aerosols that are influenced by changed anthropogenic emissions. The aerosol emission data used in the models are described in Lamarque et al. (2010). No models used in this study include parameterizations for nitrate aerosols, although studies have shown that the global mean AOD is more precise when nitrate and secondary organic aerosols (SOA) are included (Shindell et al., 2013).

5 Sulfate and sea salt particles are reflecting and hygroscopic whereas carbonaceous aerosols are generally absorbing and non hygroscopic. Therefore, the main contribution to cloud albedo variations within and between the experiments is expected to be caused by sulfate aerosols. All models used in this study include parameterizations for the cloud albedo effect (Ekman, 2014; Takemura et al., 2005). The parameterizations differ widely, from a simplified scheme with a log-linear relationship between aerosol concentration and cloud droplet number concentration (CDNC), e.g. Quaas and Boucher (2005), or with
10 higher complexity where CDNC is dependent on aerosol concentration, size, composition and supersaturation, e.g. Abdul-Razzak and Ghan (2000). The cloud lifetime effect is included in all models, except one (see Table 1).

Six GCMs in the CMIP5 archive provided the required output for all three experiments (see Table 1), giving the total cloud fraction, top of the atmosphere upwelling and downwelling shortwave radiation fluxes and AOD as monthly means. We study 30 years of output from each simulation. Our analysis focuses on five regions of low marine stratocumulus clouds, following
15 Klein and Hartmann (1993); Australian (25-35°S, 95-105°E), Californian (20-30° N, 120-130°W), Canarian (15-25°N, 25-35°W), Namibian (10-20°S, 0-10°E) and Peruvian (10-20°S, 80-90°W). The total albedo is calculated as the upwelling divided by the downwelling shortwave radiation flux. Following Bender et al. (2016), the model output is de-seasonalized and also de-regionalized, i.e. we study deviations from the mean annual signature and the mean geographical signature in each region. This is done to capture AOD-related variations in cloud albedo independent of time and location, relative to any large-scale seasonal
20 or geographical patterns, such as for instance off-shore gradients of aerosol and cloud in the Peruvian region (Wyant et al., 2015). In agreement with Bender et al. (2016) who found that a correlation between AOD and cloud fraction masked the cloud brightening signal in satellite observations, the AOD anomaly is used in Sect. 3.3, instead of the absolute AOD. To obtain the AOD anomaly, the mean is subtracted from the AOD for each given cloud fraction.

3 Results and discussion

25 3.1 Global distribution of AOD changes

Previous studies, notably the model-intercomparison performed by Shindell et al. (2013) within the ACCMIP (Atmospheric Chemistry and Climate Model Intercomparison Project, Lamarque et al. (2013)) have found a general agreement with observations in terms of total AOD, but pointed at model underestimates particularly over East Asia and Europe, and large inter-model differences.

30 In the present study, the All Aerosol experiment, where all aerosols are at a level corresponding to year 2000, is taken as a representation of the present-day aerosol distribution. Four of the models utilized (CSIRO, HadGEM, IPSL, MIROC) are also included in the earlier ACCMIP, and examination of the All Aerosol total AOD (not shown) confirms the results of Shindell



et al. (2013). In addition, it is found that NorESM underestimates the AOD especially in South Asia (also shown by Kirkevåg et al. (2013)), and that MRI (Yukimoto et al., 2012) underestimates the global total AOD (not shown).

To map changes in AOD due to different types of anthropogenic aerosols we analyze the spatial distribution of the 550 nm AOD differences between the Control and sensitivity experiments described in Sect. 2. Figure 1 shows relative changes due to changes from preindustrial to present-day levels of all anthropogenic aerosols, sulfate and non-sulfate aerosols, respectively, for all models. A general increase in total AOD due to the changes in aerosol emissions can be seen for the All Aerosol experiment (Fig. 1a), with a pattern representing the combination of those from sulfate and non-sulfate aerosol increases (Fig. 1b and c). Due to short aerosol life time, the distribution of AOD differences largely reflects the emission sources of anthropogenic aerosols. The main biomass burning regions cause increases in non-sulfate aerosols over central Africa, South America and Southeast Asia. Industrial pollution by sulfate aerosols is high over Europe, North America and Southeast Asia. The regions of stratocumulus cloud maxima, marked with boxes in Fig. 1, in most cases do not overlap with the maximum changes in AOD, but for the All Aerosol case (Fig. 1a) significant increases in AOD are seen in all studied regions and models, except for the Canarian region in MIROC and the Australian region in HadGEM, MIROC and MRI. The focus regions in the southern hemisphere are in general more influenced by non-sulfate aerosols while the regions in the northern hemisphere are dominated by sulfate aerosols, in agreement with previous studies (e.g. Ramanathan et al. (2001)). For NorESM, the BC Only experiment indicates that increases in AOD due to BC are comparatively small, and in some cases counteracted by decreases in OM, particularly in the Californian region, as seen from the difference between Fig. 1c and d.

IPSL shows the largest AOD change in all regions, whereas HadGEM shows the smallest changes. MIROC shows negative deviations in the Canarian region, but without statistical significance, consistent with high variability of background aerosol in that region. Decreased AOD in large parts of North America in the Non Sulfate case are related to decreases in OM emissions, cf. Bond et al. (2007); Lamarque et al. (2010).

The AOD is not available for separated aerosol types from the CMIP5 archive. However, analysis of the loading of individual aerosol types can give an indication of the aerosol types dominating the variability in total AOD in the different regions. The aerosol loading is a mass measure for the amount of aerosols in a vertical column of the atmosphere and is given in units of kgm^{-2} . The relative aerosol loading contributions for all models for the different regions in the Control simulation are listed in Table 2. The mass loading in all regions is dominated by dust and sea salt, consistent with these aerosol types forming primarily large and heavy particles. In the Canarian region, the dust loading is between 70 and 90 % of the total aerosol loading. The BC mass loading is negligible compared to other aerosol types for all regions and models. NorESM consistently shows a larger fraction of OM than the other models, and NorESM and CSIRO in general have higher fractions of sulfate contribution to the total loading, compared to the other models.

The correlation coefficient (temporal and spatial) between AOD and loading of different aerosol types is listed in Table 3. It is clear that in the Canarian region, the AOD variability is dominated by variability in dust aerosol, with correlation coefficients above 0.9 for all models. Dust aerosol also explains the largest part of the variance in AOD in the Australian region for CSIRO and HadGEM, whereas in the other models sea salt variability dominates. For the Californian region, where Fig. 1 shows that AOD changes due to anthropogenic sulfate are large, sulfate becomes important for explaining the variance in AOD in most



models, but in most cases several aerosol types contribute to the variability. For the biomass burning affected Namibian and Peruvian regions, where BC and other non-sulfate aerosols contribute mostly to the anthropogenic AOD change according to Fig. 1, BC and OM are in most models important for explaining the variance in total AOD, together with sulfate and dust and to some extent sea salt. For MRI however, neither BC or OM loading correlates well with the total AOD in the biomass burning regions, and sea salt explains most of the AOD variance in all cases except the dust-dominated Canarian region.

3.2 AOD Variability

The absolute AOD, and its variability varies among regions and models, as seen in Figure 2.

The year 2000 emissions, used in the All Aerosol experiments, are expected to be representative for the period 2002-2015 and model results can thus be compared with MODIS satellite observations. Figure 2 shows that CSIRO overestimates and MIROC underestimates the AOD compared to observations in all regions, and MRI overestimates AOD except in the Australian region. HadGEM, IPSL and NorESM are generally in closest agreement with the observations, although HadGEM overestimates AOD and variability in the Australian region, consistent with an overestimation of dust loading in this area (Bellouin et al., 2011).

MIROC and MRI show the best agreement with observations in terms of variability, whereas the other models overestimate the variability. For the Canarian region, all models show too large variability compared to observations. The variability is overall largest for CSIRO, but HadGEM shows the largest variability in the Australian region, as noted above.

These results are overall consistent with previous study results on the global scale, where HadGEM agrees well with observations, IPSL and MIROC underestimate the mean AOD and CSIRO overestimates the AOD compared to observations (Shindell et al., 2013).

As expected, the All Aerosol experiment where all anthropogenic aerosol emissions from the year 2000 are added, display the highest AOD values. The median AOD and AOD variability is considerably higher in the Canarian region, where AOD is dominated by dust (see Sect. 3.1) than in the other regions.

The Control experiment shows a similar variability as the All Aerosol experiment in all regions, indicating a high variability of the preindustrial background aerosol and only a slight increase in variability caused by added anthropogenic aerosols. The variability in the Non Sulfate case is typically larger than that of the Sulfate Only case, indicating that the added variability from anthropogenic aerosol increases comes primarily from non-sulfate aerosols. De-seasonalizing the time series (as described in Sect. 2) has little effect on the variability range, i.e. the seasonal pattern of variation is not a main contributor to the AOD variability in these regions (not shown).

We note that the regional mean change in AOD between experiments, i.e. due to the addition of anthropogenic aerosol emissions, is typically small compared to the total spatio-temporal variability in AOD within the individual experiments, shown in Fig. 2. For the Canarian region the background variability greatly exceeds the AOD difference between experiments for all models, whereas for the other regions the AOD change is of similar magnitude as the interquartile range in AOD in the models with smallest variability.



3.3 Cloud albedo and cloud brightening effect

As described in Sect. 1, an aerosol-induced cloud brightening on the month-to-month scale can be determined by the variation of the AOD anomaly with the albedo at a given cloud fraction. We will refer to this variation as an AOD anomaly gradient, where a positive gradient means that the albedo at a given cloud fraction is higher for a higher AOD, and vice versa for a negative gradient. Figure 3 in this way depicts the AOD anomaly in the albedo-cloud fraction space for all experiments for NorESM in the Californian region, as an example. To quantify the direction and strength of the emerging gradient, two separate linear regressions are performed for the points falling above the 90th and below the 10th percentile of the AOD anomaly range respectively. The two separate regression lines are indicated in Fig. 3, and the difference between the derived cloud albedo for the upper and lower regression lines is given as the gradient strength. Figure 4 summarizes the gradient strengths for all regions, all experiments and all models.

A predominantly positive AOD gradient appears for all models in the five regions for the All Aerosol experiment, in agreement with what Bender et al. (2016) found for present-day simulations for a larger set of CMIP5 models. One model, CSIRO, in contrast shows a weak negative gradient for the Namibian region. For the Control experiment, the cloud albedo also co-varies with aerosols and positive gradients are seen, which indicates that a cloud brightening on month-to-month scale also occurs due to preindustrial aerosols only. For the Namibian and Peruvian regions there are cases of negative gradients.

Comparing the gradient strengths (Fig. 4), there is no systematic strengthening of the AOD gradient between the Control and All Aerosol experiments, which supports the idea that month-to-month scale cloud brightening by preindustrial aerosols is similar in strength to that induced by total (preindustrial and anthropogenic) aerosols. This is also in agreement with the relatively small difference in variability between the Control and All Aerosol experiments found in Sect. 3.2. In most models, both the Sulfate Only and the Non Sulfate cases show positive gradients, again consistent with the background aerosol, rather than the added anthropogenic aerosols, being largely responsible for the gradient. For CSIRO in the Namibian region, the gradients in the Control and Sulfate Only cases are clearly positive, but in both the Non Sulfate and All Aerosol cases weaker, or negative. This is consistent with the increased non-sulfate aerosol counteracting the background cloud brightening on the month-to-month scale.

The gradients are overall weakest for the Namibian region, where BC and OM are typically important for explaining the AOD variability, consistent with absorbing aerosol counteracting the cloud brightening, as suggested by Bender et al. (2016). The positive gradients are on the other hand strongest in the dust-dominated Canarian region, where satellite observations indicate negative gradients (Bender et al., 2016). The aerosol composition appears to be more important for the gradient strength than the total AOD variability; the Canarian region has the largest AOD variability, but the Namibian region also typically shows higher variability than the remaining regions (see Fig. 2).

As described in Sect. 2, the cloud albedo for each model, region and experiment, can be estimated from a linear regression for the linear relation between cloud fraction and albedo. The deviation in cloud albedo between the sensitivity experiments and Control simulation shows, that the cloud albedo is enhanced due to increased anthropogenic aerosol emissions for most of the models and regions (see Fig. 5). In agreement with Zelinka et al. (2014), both sulfate and non-sulfate aerosols enhance



the cloud albedo in general, but the increase in cloud albedo is typically larger for sulfate than non-sulfate aerosols. In the Australian region several models indicate decreased cloud albedo due to changes in non-sulfate aerosol, but as seen in Sect. 3.1, the AOD changes due to non-sulfate aerosol are small and rarely significant.

Previous studies have shown that aerosol forcings are not necessarily linearly additive (Stier et al., 2006; Jones et al., 2007), but here the sum of the effects of anthropogenic sulfate and non-sulfate aerosols on the cloud albedo is within the uncertainty range of the effect of all anthropogenic aerosols, in most cases.

The highest cloud albedo change is found in the Californian and Canarian regions in agreement with Engström et al. (2014), as opposed to the Australian region with the lowest cloud albedo changes. The latter region is more influenced by non-sulfate aerosols in contrast with the regions in the northern hemisphere which are more influenced by sulfate aerosols (see Sect. 3.1). The greatest model diversity in terms of cloud albedo response also occurs in the Californian and Canarian regions, whereas in the Australian, Namibian and Peruvian regions the model agreement is better. MIROC, which has a prognostic CDNC scheme shows small cloud albedo changes in all regions, but on the other hand in MRI and NorESM, which also have prognostic CDNC schemes, the cloud albedo changes are in some cases large. IPSL, which is the only model that does not include a cloud lifetime effect, shows comparatively small changes in cloud albedo, consistent with (Zelinka et al., 2014) who found a low effective radiative forcing due to aerosol-cloud interactions for this model compared to other CMIP5 models.

Even though the cloud albedo changes in the five regions are small, within 0.03, the aerosol changes have a substantial local radiative effect. The difference in upwelling shortwave radiation between the All Aerosol and Control experiments, i.e. the total radiative effect due to changes in both cloud fraction, cloud albedo and clear-sky albedo caused by anthropogenic aerosols, are as large as -6.0 W m^{-2} in the Californian region. The largest changes in radiation occur in the Californian and Canarian regions, consistent with the larger cloud albedo changes, and MRI and HadGEM show the greatest changes in shortwave radiation, also in agreement with their higher cloud albedo change.

To investigate what controls the sensitivity of changes in cloud albedo due to anthropogenic aerosols in this set of models, we analyze relations between cloud albedo change and potential explaining factors.

It has been suggested that for a given change in sulfate loading, the magnitude of the cloud albedo effect should be larger for models with low preindustrial loading, due to cloud droplet size being more sensitive to changes in sulfate loading at low loadings (Carslaw et al., 2013; Wilcox et al., 2015). However, as sulfate loading change as well as preindustrial sulfate loading vary among the models studied here, we find no general relationship between sulfate loading or sulfate loading change and cloud albedo change. For the primary biomass burning regions, there is a tendency for models with larger change in sulfate load to show smaller change in cloud albedo between the Control and All Aerosol experiments (correlation coefficients are 0.89 and 0.81, significant at the 90% level, for the Namibian and Peruvian regions respectively), see Fig. 6. Assuming that the sulfate increase in these regions scales with the BC increase, this is consistent with increases in absorbing aerosol counteracting cloud brightening. However, there is no detectable correlation between total AOD change and cloud albedo change among the models in any of the regions (not shown).

Turning to gradient strength, IPSL that has the weakest gradient strengths overall, also shows small changes in cloud albedo, and MRI that has strong positive gradients also in general shows large differences in cloud albedo between experiments (cf.



Fig. 4 and 5). However, overall the AOD anomaly gradient strength is not well correlated with the cloud albedo change (not shown), suggesting that models with stronger cloud brightening effect on the month-to-month scale do not necessarily have a stronger cloud albedo effect due to anthropogenic aerosol changes.

As cloud albedo is strongly dependent on LWP, we also examine the change in LWP between experiments. From the experiment setup of the fixed SST simulations, only small changes in LWP are expected, due to small changes in the land temperature which can affect the circulation and thereby cloud properties (Erickson et al., 1995; Hansen et al., 2005; Allen and Sherwood, 2010; Lewinschal et al., 2012). But all models, except one, include the cloud lifetime effect, i.e. higher aerosol concentrations in the sensitivity experiments leading to smaller and more cloud droplets and thereby reducing the precipitation efficiency and increasing the LWP. An increase in LWP leads to a higher cloud albedo, which can enhance the cloud brightening by the Twomey effect. Total changes in LWP between experiments (circulation and aerosol driven) are typically positive, and in most regions also positively correlated with the change in cloud albedo. For the Namibian region no significant correlation can be detected, but for the Australian, Californian, Canarian and Peruvian regions correlation coefficients are 0.3 (80% significance), 0.7 (95% significance), 0.4 (90% significance) and 0.6 (95% significance) respectively, see Fig. 7.

In summary, the strength of the month-to-month cloud brightening seems to be less important for the cloud albedo change due to anthropogenic aerosol than the change in LWP that follows the aerosol forcing. We also note that the changes in LWP between experiments make it difficult to isolate the cloud albedo effect, which in theory acts at constant LWP.

3.4 Vertical aerosol and cloud distributions

Absorbing aerosols overlying low clouds may cause a scene darkening. This was suggested by Bender et al. (2016) as an explanation for high AOD being related to low albedo for a given cloud fraction, as was indicated by satellite data for the Canarian and Namibian stratocumulus regions. As in the historical CMIP5 simulations discussed by Bender et al. (2016), the model simulations studied here with few exceptions display positive gradients, but it is still of interest to examine the vertical distribution of clouds and aerosols in these models, to investigate if they have any relation to the gradient direction and strength.

Vertically resolved aerosol extinction, which can be integrated over the atmospheric column to yield the total AOD, is only available for three models (MIROC, IPSL and NorESM) in the CMIP5 archive. All three models show an aerosol layer above the low clouds in the Canarian region, consistent with observations (Chand et al., 2008; Devasthale and Thomas, 2011; Waquet et al., 2013; Winker et al., 2013), with a contribution of 50% to the total AOD. Figure 8 shows vertical cross sections of the aerosol extinction coefficient at 550 nm and the vertically resolved cloud fraction for the model MIROC, in the Canarian region, as an example, and an aerosol layer co-located with the cloud layer as well as an overlying aerosol layer is evident for all four experiments. The overlying aerosols here are assumed to be dust aerosols as the dominant loading type is dust in the Canarian region. Dust aerosols are parameterized as weakly absorbing in the models and could hence reduce the scene albedo. MIROC however, shows positive gradients in the Canarian region (cf. Fig 4), although somewhat weaker than for other regions, especially in the Non Sulfate case. NorESM has distinct positive gradients in the Canarian region. The strongest negative gradient (Fig. 4) is seen for MIROC in the Namibian region, where overlying aerosols are found only for parts of the year, not affecting the annual mean. On the whole, there is no indication of systematic presence of overlying aerosol in the



regions where weak or negative gradients are seen. Hence, to the extent that overlying aerosols occur in these models, they are not sufficiently absorbing to overcome the cloud brightening and create negative AOD gradients, as those seen in satellite data (Bender et al., 2016), and there is no clear dependence of gradient strength on overlying aerosol.

MRI overall has strong AOD gradients and large sensitivity, and is also one of the models that include aerosol interactions with ice clouds (Rotstayn et al., 2013). An analysis of the vertical cloud fraction shows that for MRI in the Californian region, high clouds frequently occur above the low clouds, and enhanced cloud albedo from high clouds could therefore increase the total albedo and contribute to scene brightening. However, the Californian region does not stand out as more sensitive than other regions, with less high cloud occurrence. For MIROC, that also includes aerosol interaction with ice clouds (Rotstayn et al., 2013), high clouds are seen in the Namibian region, where gradients are found to be negative. Hence, ice cloud interaction does not seem to be important for the total effect of aerosol on cloud albedo, and the predefined regions in general contain mainly low clouds, in agreement with what is seen in satellite observations (Bender et al., 2016).

3.5 Black carbon influence on the cloud albedo

For NorESM an additional BC Only experiment was carried out. The largest changes in AOD due to BC aerosols can be seen in the biomass burning regions in South America, equatorial Africa and Southeast Asia, see Fig. 1. The vertical distribution of BC aerosols is important for the radiative forcing in models (Samset et al., 2013) in general, and strongly absorbing BC aerosols above marine stratocumulus clouds could potentially darken the scene and lower the albedo, but as discussed in Sect. 3.4, there are no overlying aerosols above the cloud layer in the main regions of BC loading, the Namibian and Peruvian region, in the model simulations studied here.

The AOD gradient reflecting month-to-month-cloud brightening for the BC Only experiment is shown in Fig. 3 for the Californian region, and gradient strengths for all regions are summarized in Fig. 4. In the Peruvian and Namibian regions where the BC loading is high, the gradients are weaker or reversed, compared to the Non Sulfate case, where BC as well as OM is increased, indicating that the BC may actually have an effect of counteracting and dampening the cloud brightening. In the other regions the gradients remain positive, which supports the idea, that the natural background aerosol causes a cloud brightening that the additional BC can not counteract. It is noteworthy that relative AOD changes due to increased BC emissions on the global scale are tenfold smaller than due to all non-sulfate aerosols (Fig. 1), but it is also noteworthy that absorption by BC is commonly underestimated in models, (Bond et al., 2013), suggesting that the dampening of the cloud brightening could in fact be underestimated.

4 Conclusions

The aim of this study is to determine the effects of different aerosol types on the cloud albedo in an ensemble of climate models. Six CMIP5 models provided output from sensitivity experiments where total and sulfate-only aerosol emissions were separately changed to present-day levels, while all other anthropogenic forcings were kept at a preindustrial level. The models all parameterize the cloud albedo effect, i.e. higher aerosol concentration leading to an increase of the cloud droplet number



concentration and a decrease of droplet size at constant liquid water content, with a resulting increase in cloud albedo with increasing amount of aerosol. We use the methods of Bender et al. (2011, 2016) to examine the relation between AOD and cloud albedo in five marine subtropical stratocumulus regions, separating the effects of anthropogenic sulfate and non-sulfate aerosols from the preindustrial background aerosols.

- 5 The representation of the AOD and its change from preindustrial to present-day conditions, shows large differences between the models confirming results from previous studies (Shindell et al., 2013). An increased AOD, due to changed emissions, can be identified in the five study regions for almost all models. The Canarian and Australian regions are less influenced by anthropogenic aerosols than the other regions, and particularly the Canarian region is largely dust-dominated. The Californian region is mainly influenced by sulfate aerosols while the Namibian and Peruvian regions are dominated by non-sulfate aerosols.
- 10 The addition of anthropogenic aerosols only slightly increases the AOD variability from that of the background state, and the variability increases more due to addition of non-sulfate than sulfate aerosols.

A general co-variation between cloud albedo and AOD is found, represented by a positive gradient in AOD anomaly in albedo-cloud fraction space, indicating an aerosol-related cloud brightening on the month-to-month scale. Similar signals have been found in simulations of present-day climate (Bender et al., 2016), but here positive gradients are found not only in the presence of all anthropogenic aerosols, but also in the reference experiment with aerosols at preindustrial level, and when sulfate and non-sulfate aerosols only are increased. Only a slight strengthening of the dependence occurs with additional anthropogenic aerosols compared to the case with preindustrial conditions, which supports the notion of a cloud brightening effect by background aerosols. Previous studies, e.g. Carslaw et al. (2013) have also shown that the albedo sensitivity to CCN is higher in clean preindustrial conditions with low CDNC compared to present-day conditions.

- 20 The month-to-month scale cloud brightening is generally greatest for the dust-dominated Canarian region, whereas the weakest cloud brightening signals and the most instances of reversal of the AOD anomaly gradient are seen in the more BC-dominated Namibian and Peruvian regions, particularly in an additional experiment isolating BC aerosol increases.

The aerosol composition is hence of importance for the gradient strength, but the cloud brightening shows no clear dependence on the vertical distribution of the aerosols. Dust aerosols above the clouds are found in the Canarian region, but BC aerosols are not found to be prevalent above the clouds in the biomass burning regions, which may be expected from observations (Chand et al., 2008; Devasthale and Thomas, 2011; Waquet et al., 2013; Winker et al., 2013), and which may further counteract the cloud brightening. Hence, the darkening effect of the anthropogenic non-sulfate aerosols is not strong enough in the models to counteract the brightening effect of the background aerosol, leaving climate models with predominantly positive gradients in disagreement with satellite observations (Bender et al., 2016).

- 30 However, the strength of the month-to-month cloud brightening does not seem to be critical for the magnitude of the cloud albedo change between experiments. The regional mean cloud albedo is estimated for the different forcing scenarios, based on the near-linear relation between albedo and cloud fraction. An enhanced cloud albedo due to addition of both anthropogenic sulfate and non-sulfate aerosols is found, consistent with Zelinka et al. (2014), but sulfate aerosols tend to cause a larger increase in cloud albedo than non-sulfate aerosols. The sum of the cloud albedo changes due to sulfate and non-sulfate aerosols are within the uncertainty ranges of the changes due to all aerosols. The cloud albedo increases are typically larger for the
- 35



regions in the northern hemisphere, consistent with the dominance of sulfate aerosols in these regions. We note however, that the change in AOD between experiments is typically small compared to the AOD variability within experiments; this is true for all models in the Canary region, and for most models in the remaining four regions. Models with stronger cloud brightening on the month-to-month scale do not show systematically higher cloud albedo change with addition of anthropogenic aerosols. This means that the discrepancy between models and observations in terms of cloud brightening on month-to-month scale does not necessarily have consequences for the effective radiative forcing due to aerosol-cloud interactions.

The spread in cloud albedo change in this ensemble of models can not be related to differences in pre-industrial sulfate loading or parameterizations of the CDNC, which has been found important in previous studies (Penner et al., 2006; Storelvmo et al., 2009; Wilcox et al., 2015). Among models with a prognostic CDNC scheme (NorESM, MIROC, MRI) some are more and some less sensitive to aerosol changes compared to models with a diagnostic scheme. Similarly, the models MIROC and MRI that include aerosol interaction with ice clouds (Rotstayn et al., 2013) can not be singled out in terms of cloud albedo sensitivity in these stratocumulus-dominated regions, although ice cloud effects have been found to be important for radiative forcing due to aerosol-cloud interaction on global scale (Zelinka et al., 2014).

Rather, the change in regional mean cloud albedo induced by the addition of anthropogenic aerosols seems to be primarily driven by changes in LWP between the experiments. These changes may be induced by aerosol interaction with the clouds through the cloud lifetime effect, by which more aerosol particles leads to smaller droplets and reduced precipitation efficiency, or by aerosol forcing causing changes in circulation that affect the cloud properties indirectly (Erickson et al., 1995; Hansen et al., 2005; Allen and Sherwood, 2010; Lewinschal et al., 2012). This elucidates the difficulty of isolating aerosol effects on clouds from meteorological variations (Stevens and Feingold, 2009; Engström and Ekman, 2013; Peters et al., 2014; Rosenfeld et al., 2014; Feingold et al., 2016) not only in observations, but also in models.

5 Code availability

Code will be provided from the corresponding author upon request.

6 Data availability

The used CMIP5 data is available through <https://pcmdi.llnl.gov/search/cmip5/>.

Competing interests. The authors declare that they have no conflict of interest.

Acknowledgements. We acknowledge the World Climate Research Programme's Working Group on Coupled Modelling, which is responsible for CMIP, and we thank the climate modeling groups (listed in Table 1 of this paper) for producing and making available their model output. For CMIP the U.S. Department of Energy's Program for Climate Model Diagnosis and Intercomparison provides coordinating support and led development of software infrastructure in partnership with the Global Organization for Earth System Science Portals.



References

- Abdul-Razzak, H. and Ghan, S. J.: A parameterization of aerosol activation: 2. Multiple aerosol types, *J. Geophys. Res. Atmos.*, 105, 6837–6844, doi:10.1029/1999JD901161, 2000.
- Ackerman, A. S., Toon, O. B., Stevens, D. E., Heymsfield, A. J., Ramanathan, V., and Welton, E. J.: Reduction of tropical cloudiness by soot, *Science*, 288, 1042–1047, doi:10.1126/science.288.5468.1042, 2000.
- Albrecht, B. A.: Aerosols, Cloud Microphysics, and Fractional Cloudiness, *Science*, 245, 1227–1230, doi:10.1126/science.245.4923.1227, 1989.
- Allen, R. J. and Sherwood, S.: The impact of natural versus anthropogenic aerosols on atmospheric circulation in the Community Atmosphere Model, *Clim. Dynam.*, 36, 1959–1978, doi:10.1007/s00382-010-0898-8, 2010.
- Andreae, M. O.: Correlation between cloud condensation nuclei concentration and aerosol optical thickness in remote and polluted regions, *Atmos. Chem. Phys.*, 9, 543–556, doi:10.5194/acp-9-543-2009, 2009.
- Bellouin, N., Boucher, O., Haywood, J., Johnson, C., Jones, A., Rae, J., and Woodward, S.: Improved representation of aerosols for HadGEM2, vol. 73, Met Office Hadley Centre, Exeter, U.K., 2007.
- Bellouin, N., Rae, J., Jones, A., Johnson, C., Haywood, J., and Boucher, O.: Aerosol forcing in the Climate Model Intercomparison Project (CMIP5) simulations by HadGEM2-ES and the role of ammonium nitrate, *J. Geophys. Res. Atmos.*, 116, doi:10.1029/2011JD016074, d20206, 2011.
- Bender, F. A.-M., Rodhe, H., Charlson, R. J., Ekman, A. M. L., and N, L.: 22 views of the global albedo—comparison between 20 GCMs and two satellites, *Tellus A*, 58, 320–330, doi:10.1111/j.1600-0870.2006.00181.x, 2006.
- Bender, F. A.-M., Charlson, R. J., Ekman, A. M. L., and Leahy, L. V.: Quantification of Monthly Mean Regional-Scale Albedo of Marine Stratiform Clouds in Satellite Observations and GCMs, *J. Appl. Meteorol. Climatol.*, 50, 2139–2148, doi:10.1175/JAMC-D-11-049.1, 2011.
- Bender, F. A.-M., Engström, A., and Karlsson, J.: Factors controlling cloud albedo in marine subtropical stratocumulus regions in climate models and satellite observations, *J. Clim.*, 29, 3559–3587, doi:10.1175/JCLI-D-15-0095.1, 2016.
- Bond, T. C., Bhardwaj, E., Dong, R., Jogani, R., Jung, S., Roden, C., Streets, D. G., and Trautmann, N. M.: Historical emissions of black and organic carbon aerosol from energy-related combustion, 1850–2000, *Global Biogeochem. Cycles*, 21, doi:10.1029/2006GB002840, gB2018, 2007.
- Bond, T. C., Doherty, S. J., Fahey, D. W., Forster, P. M., Berntsen, T., DeAngelo, B. J., Flanner, M. G., Ghan, S., Kärcher, B., Koch, D., Kinne, S., Kondo, Y., Quinn, P. K., Sarofim, M. C., Schultz, M. G., Schulz, M., Venkataraman, C., Zhang, H., Zhang, S., Bellouin, N., Guttikunda, S. K., Hopke, P. K., Jacobson, M. Z., Kaiser, J. W., Klimont, Z., Lohmann, U., Schwarz, J. P., Shindell, D., Storelvmo, T., Warren, S. G., and Zender, C. S.: Bounding the role of black carbon in the climate system: A scientific assessment, *J. Geophys. Res. Atmos.*, 118, 5380–5552, doi:10.1002/jgrd.50171, 2013.
- Bony, S. and Dufresne, J.-L.: Marine boundary layer clouds at the heart of tropical cloud feedback uncertainties in climate models, *Geophys. Res. Lett.*, 32, doi:10.1029/2005GL023851, l20806, 2005.
- Boucher, O., Randall, D., Artaxo, P., Bretherton, C., Feingold, G., Forster, P., Kerminen, V.-M., Kondo, Y., Liao, H., and Lohmann, U.: Clouds and aerosols, in: *Clim. Chang. 2013 Phys. Sci. basis. Contrib. Work. Gr. I to fifth Assess. Rep. Intergov. panel Clim. Chang.*, pp. 571–657, Cambridge University Press, 2013.



- Carslaw, K. S., Lee, L. A., Reddington, C. L., Pringle, K. J., Rap, A., Forster, P. M., Mann, G. W., Spracklen, D. V., Woodhouse, M. T., Regayre, L. A., and Pierce, J. R.: Large contribution of natural aerosols to uncertainty in indirect forcing, *Nature*, 503, 67–71, doi:10.1038/nature12674, 2013.
- Chand, D., Anderson, T. L., Wood, R., Charlson, R. J., Hu, Y., Liu, Z., and Vaughan, M.: Quantifying above-cloud aerosol using spaceborne lidar for improved understanding of cloudy-sky direct climate forcing, *J. Geophys. Res. Atmos.*, 113, doi:10.1029/2007JD009433, d13206, 2008.
- Collins, W. J., Bellouin, N., Doutriaux-Boucher, M., Gedney, N., Halloran, P., Hinton, T., Hughes, J., Jones, C. D., Joshi, M., Liddicoat, S., Martin, G., O'Connor, F., Rae, J., Senior, C., Sitch, S., Totterdell, I., Wiltshire, A., and Woodward, S.: Development and evaluation of an Earth-System model – HadGEM2, *Geosci. Model Dev.*, 4, 1051–1075, doi:10.5194/gmd-4-1051-2011, 2011.
- Devasthale, A. and Thomas, M. A.: A global survey of aerosol-liquid water cloud overlap based on four years of CALIPSO-CALIOP data, *Atmos. Chem. Phys.*, 11, 1143–1154, doi:10.5194/acp-11-1143-2011, 2011.
- Dufresne, J.-L., Foujols, M.-A., Denvil, S., Caubel, A., Marti, O., Aumont, O., Balkanski, Y., Bekki, S., Bellenger, H., Benshila, R., Bony, S., Bopp, L., Braconnot, P., Brockmann, P., Cadule, P., Cheruy, F., Codron, F., Cozic, A., Cugnet, D., Noblet, N., Duvel, J.-P., Ethé, C., Fairhead, L., Fichefet, T., Flavoni, S., Friedlingstein, P., Grandpeix, J.-Y., Guez, L., Guilyardi, E., Hauglustaine, D., Hourdin, F., Idelkadi, A., Ghattas, J., Joussaume, S., Kageyama, M., Krinner, G., Labetoulle, S., Lahellec, A., Lefebvre, M.-P., Lefevre, F., Levy, C., Li, Z. X., Lloyd, J., Lott, F., Madec, G., Mancip, M., Marchand, M., Masson, S., Meurdesoif, Y., Mignot, J., Musat, I., Parouty, S., Polcher, J., Rio, C., Schulz, M., Swingedouw, D., Szopa, S., Talandier, C., Terray, P., Viovy, N., and Vuichard, N.: Climate change projections using the IPSL-CM5 Earth System Model: from CMIP3 to CMIP5, *Clim. Dyn.*, 40, 2123–2165, doi:10.1007/s00382-012-1636-1, 2013.
- Ekman, A. M. L.: Do sophisticated parameterizations of aerosol-cloud interactions in CMIP5 models improve the representation of recent observed temperature trends ?, *J. Geophys. Res. Atmos.*, 119, 817–832, doi:10.1002/2013JD020511, 2014.
- Engström, A. and Ekman, A. M. L.: Impact of meteorological factors on the correlation between aerosol optical depth and cloud fraction, *Geophys. Res. Lett.*, 37, doi:10.1029/2010GL044361, 118814, 2013.
- Engström, A., Bender, F. A.-M., and Karlsson, J.: Improved Representation of Marine Stratocumulus Cloud Shortwave Radiative Properties in the CMIP5 Climate Models, *J. Clim.*, 27, 6175–6188, doi:10.1175/JCLI-D-13-00755.1, 2014.
- Erickson, D. J., Oglesby, R. J., and Marshall, S.: Climate response to indirect anthropogenic sulfate forcing changes, *Geophys. Res. Lett.*, 22, 2017–2020, doi:10.1029/95GL01660, 1995.
- Feingold, G., McComiskey, A., Yamaguchi, T., Johnson, J. S., Carslaw, K. S., and Schmidt, K. S.: New approaches to quantifying aerosol influence on the cloud radiative effect, *Proc. Natl. Acad. Sci.*, 113, 5812–5819, doi:10.1073/pnas.1514035112, 2016.
- Hansen, J., Sato, M., Ruedy, R., Nazarenko, L., Lacis, A., Schmidt, G. A., Russell, G., Aleinov, I., Bauer, M., Bauer, S., Bell, N., Cairns, B., Canuto, V., Chandler, M., Cheng, Y., Del Genio, A., Faluvegi, G., Fleming, E., Friend, A., Hall, T., Jackman, C., Kelley, M., Kiang, N., Koch, D., Lean, J., Lerner, J., Lo, K., Menon, S., Miller, R., Minnis, P., Novakov, T., Oinas, V., Perlwitz, J., Perlwitz, J., Rind, D., Romanou, A., Shindell, D., Stone, P., Sun, S., Tausnev, N., Thresher, D., Wielicki, B., Wong, T., Yao, M., and Zhang, S.: Efficacy of climate forcings, *J. Geophys. Res. Atmos.*, 110, doi:10.1029/2005JD005776, d18104, 2005.
- Hartmann, D., Ockert-Bell, M., and Michelsen, M.: The effect of cloud type on Earth's energy balance: global analysis, *J. Clim.*, 5, 1281–1304, doi:10.1175/1520-0442(1992)005<1281:TEOCTO>2.0.CO;2, 1992.
- Iversen, T., Bentsen, M., Bethke, I., Debernard, J. B., Kirkevåg, A., Seland, Ø., Drange, H., Kristjansson, J. E., Medhaug, I., Sand, M., and Seierstad, I. a.: The Norwegian Earth System Model, NorESM1-M – Part 2: Climate response and scenario projections, *Geosci. Model Dev.*, 6, 389–415, doi:10.5194/gmd-6-389-2013, 2013.



- Jones, A., Haywood, J. M., and Boucher, O.: Aerosol forcing, climate response and climate sensitivity in the Hadley Centre climate model, *J. Geophys. Res. Atmos.*, 112, doi:10.1029/2007JD008688, d20211, 2007.
- Karlsson, J., Svensson, G., and Rodhe, H.: Cloud radiative forcing of subtropical low level clouds in global models, *Clim. Dyn.*, 30, 779–788, doi:10.1007/s00382-007-0322-1, 2008.
- 5 Kirkevåg, A., Iversen, T., Seland, Ø., Hoose, C., Kristjánsson, J. E., Struthers, H., Ekman, a. M. L., Ghan, S., Griesfeller, J., Nilsson, E. D., and Schulz, M.: Aerosol–climate interactions in the Norwegian Earth System Model – NorESM1-M, *Geosci. Model Dev.*, 6, 207–244, doi:10.5194/gmd-6-207-2013, 2013.
- Klein, S. A. and Hartmann, D. L.: The Seasonal Cycle of Low Stratiform Clouds, *J. Clim.*, 6, 1587–1606, doi:10.1175/1520-0442(1993)006<1587:TSCOLS>2.0.CO;2, 1993.
- 10 Lamarque, J.-F., Bond, T. C., Eyring, V., Granier, C., Heil, A., Klimont, Z., Lee, D., Liousse, C., Mieville, A., Owen, B., Schultz, M. G., Shindell, D., Smith, S. J., Stehfest, E., Van Aardenne, J., Cooper, O. R., Kainuma, M., Mahowald, N., McConnell, J. R., Naik, V., Riahi, K., and van Vuuren, D. P.: Historical (1850–2000) gridded anthropogenic and biomass burning emissions of reactive gases and aerosols: methodology and application, *Atmos. Chem. Phys.*, 10, 7017–7039, doi:10.5194/acp-10-7017-2010, 2010.
- Lamarque, J.-F., Shindell, D. T., Josse, B., Young, P. J., Cionni, I., Eyring, V., Bergmann, D., Cameron-Smith, P., Collins, W. J., Doherty, R., Dalsoren, S., Faluvegi, G., Folberth, G., Ghan, S. J., Rumbold, L. W., Schulz, M., Skeie, R. B., Stevenson, D. S., Strode, S., Sudo, K., Szopa, S., Voulgarakis, A., and Zeng, G.: The Atmospheric Chemistry and Climate Model Intercomparison Project (ACCMIP): Overview and description of models, simulations and climate diagnostics, *Geosci. Model Dev.*, 6, 179–206, doi:10.5194/gmd-6-179-2013, 2013.
- 15 Lewinschal, A., Ekman, A. M. L., and Körnich, H.: The role of precipitation in aerosol-induced changes in northern hemisphere wintertime stationary waves, *Clim. Dynam.*, 41, 647–661, doi:10.1007/s00382-012-1622-7, 2012.
- 20 Myhre, G., Samset, B. H., Schulz, M., Balkanski, Y., Bauer, S., Berntsen, T. K., Bian, H., Bellouin, N., Chin, M., Diehl, T., Easter, R. C., Feichter, J., Ghan, S. J., Hauglustaine, D., Iversen, T., Kinne, S., Kirkevåg, A., Lamarque, J.-F., Lin, G., Liu, X., Lund, M. T., Luo, G., Ma, X., van Noije, T., Penner, J. E., Rasch, P. J., Ruiz, A., Seland, Ø., Skeie, R. B., Stier, P., Takemura, T., Tsigaridis, K., Wang, P., Wang, Z., Xu, L., Yu, H., Yu, F., Yoon, J.-H., Zhang, K., Zhang, H., and Zhou, C.: Radiative forcing of the direct aerosol effect from AeroCom Phase II simulations, *Atmos. Chem. Phys.*, 13, 1853–1877, doi:10.5194/acp-13-1853-2013, 2013a.
- 25 Myhre, G., Shindell, D., Bréon, F.-M., Collins, W., Fuglestedt, J., Huang, J., Koch, D., Lamarque, J.-F., Lee, D., Mendoza, B., et al.: Anthropogenic and natural radiative forcing, in: *Clim. Chang. 2013 Phys. Sci. basis. Contrib. Work. Gr. I to fifth Assess. Rep. Intergov. panel Clim. Chang.*, pp. 659–740, Cambridge University Press, 2013b.
- Nam, C., Bony, S., Dufresne, J.-L., and Chepfer, H.: The ‘too few, too bright’ tropical low-cloud problem in CMIP5 models, *Geophys. Res. Lett.*, 39, doi:10.1029/2012GL053421, l21801, 2012.
- 30 Penner, J. E., Quaas, J., Storelvmo, T., Takemura, T., Boucher, O., Guo, H., Kirkevåg, A., Kristjánsson, J. E., and Seland, Ø.: Model inter-comparison of indirect aerosol effects, *Atmos. Chem. Phys.*, 6, 3391–3405, doi:10.5194/acp-6-3391-2006, 2006.
- Peters, K., Quaas, J., Stier, P., and Graßl, H.: Processes limiting the emergence of detectable aerosol indirect effects on tropical warm clouds in global aerosol-climate model and satellite data, *Tellus B*, 66, doi:10.3402/tellusb.v66.24054, 2014.
- Quaas, J. and Boucher, O.: Constraining the first aerosol indirect radiative forcing in the LMDZ GCM using POLDER and MODIS satellite data, *Geophys. Res. Lett.*, 32, doi:10.1029/2005GL023850, l17814, 2005.
- Ramanathan, V., Crutzen, P. J., Kiehl, J. T., and Rosenfeld, D.: Aerosols, Climate, and the Hydrological Cycle, *Science*, 294, 2119–2124, doi:10.1126/science.1064034, 2001.



- Rosenfeld, D., Sherwood, S., Wood, R., and Donner, L.: Climate Effects of Aerosol-Cloud Interactions, *Science*, 343, 379–380, doi:10.1126/science.1247490, 2014.
- Rotstayn, L. D., Jeffrey, S. J., Collier, M. A., Dravitzki, S. M., Hirst, A. C., Syktus, J. I., and Wong, K. K.: Aerosol- and greenhouse gas-induced changes in summer rainfall and circulation in the Australasian region: a study using single-forcing climate simulations, *Atmos. Chem. Phys.*, 12, 6377–6404, doi:10.5194/acp-12-6377-2012, 2012.
- 5 Rotstayn, L. D., Collier, M. A., Chrastansky, A., Jeffrey, S. J., and Luo, J.-J.: Projected effects of declining aerosols in RCP4.5: unmasking global warming?, *Atmos. Chem. Phys.*, 13, 10 883–10 905, doi:10.5194/acp-13-10883-2013, 2013.
- Samsat, B. H., Myhre, G., Schulz, M., Balkanski, Y., Bauer, S., Berntsen, T. K., Bian, H., Bellouin, N., Diehl, T., Easter, R. C., Ghan, S. J., Iversen, T., Kinne, S., Kirkevåg, A., Lamarque, J.-F., Lin, G., Liu, X., Penner, J. E., Seland, Ø., Skeie, R. B., Stier, P., Takemura, T., Tsigaridis, K., and Zhang, K.: Black carbon vertical profiles strongly affect its radiative forcing uncertainty, *Atmos. Chem. Phys.*, 13, 2423–2434, doi:10.5194/acp-13-2423-2013, 2013.
- 10 Shindell, D. T., Lamarque, J.-F., Schulz, M., Flanner, M., Jiao, C., Chin, M., Young, P. J., Lee, Y. H., Rotstayn, L., Mahowald, N., Milly, G., Faluvegi, G., Balkanski, Y., Collins, W. J., Conley, A. J., Dalsoren, S., Easter, R., Ghan, S., Horowitz, L., Liu, X., Myhre, G., Nagashima, T., Naik, V., Rumbold, S. T., Skeie, R., Sudo, K., Szopa, S., Takemura, T., Voulgarakis, A., Yoon, J.-H., and Lo, F.: Radiative forcing in the ACCMIP historical and future climate simulations, *Atmos. Chem. Phys.*, 13, 2939–2974, doi:10.5194/acp-13-2939-2013, 2013.
- 15 Slingo, A.: Sensitivity of the Earth's radiation budget to changes in low clouds, *Nature*, 343, 49–51, doi:10.1038/343049a0, 1990.
- Stevens, B.: Rethinking the Lower Bound on Aerosol Radiative Forcing, *J. Clim.*, 28, 4794–4819, doi:10.1175/JCLI-D-14-00656.1, 2015.
- Stevens, B. and Feingold, G.: Untangling aerosol effects on clouds and precipitation in a buffered system, *Nature*, 461, 607–613, doi:10.1038/nature08281, 2009.
- 20 Stier, P., Feichter, J., Kloster, S., Vignati, E., and Wilson, J.: Emission-Induced Nonlinearities in the Global Aerosol System: Results from the ECHAM5-HAM Aerosol-Climate Model, *J. Clim.*, 19, 3845–3862, doi:10.1175/JCLI3772.1, 2006.
- Storelvmo, T., Lohmann, U., and Bennartz, R.: What governs the spread in shortwave forcings in the transient IPCC AR4 models?, *Geophys. Res. Lett.*, 36, doi:10.1029/2008GL036069, 101806, 2009.
- Takemura, T., Nozawa, T., Emori, S., Nakajima, T. Y., and Nakajima, T.: Simulation of climate response to aerosol direct and indirect effects with aerosol transport-radiation model, *J. Geophys. Res. Atmos.*, 110, doi:10.1029/2004JD005029, d02202, 2005.
- 25 Taylor, K. E., Stouffer, R. J., and Meehl, G. a.: An Overview of CMIP5 and the Experiment Design, *Bull. Am. Meteorol. Soc.*, 93, 485–498, doi:10.1175/BAMS-D-11-00094.1, 2012.
- Twomey, S.: The Influence of Pollution on the Shortwave Albedo of Clouds, *J. Atmos. Sci.*, 34, 1149–1152, doi:10.1175/1520-0469(1977)034<1149:TIOPOT>2.0.CO;2, 1977.
- 30 Waquet, F., Peers, F., Ducos, F., Goloub, P., Platnick, S., Riedi, J., Tanré, D., and Thieuleux, F.: Global analysis of aerosol properties above clouds, *Geophys. Res. Lett.*, 40, 5809–5814, doi:10.1002/2013GL057482, 2013.
- Watanabe, S., Hajima, T., Sudo, K., Nagashima, T., Takemura, T., Okajima, H., Nozawa, T., Kawase, H., Abe, M., Yokohata, T., Ise, T., Sato, H., Kato, E., Takata, K., Emori, S., and Kawamiya, M.: MIROC-ESM 2010: model description and basic results of CMIP5-20c3m experiments, *Geosci. Model Dev.*, 4, 845–872, doi:10.5194/gmd-4-845-2011, 2011.
- 35 Wilcox, L. J., Highwood, E. J., Booth, B. B. B., and Carslaw, K. S.: Quantifying sources of inter-model diversity in the cloud albedo effect, *Geophys. Res. Lett.*, 42, 1568–1575, doi:10.1002/2015GL063301, 2015.
- Winker, D. M., Tackett, J. L., Getzewich, B. J., Liu, Z., Vaughan, M. A., and Rogers, R. R.: The global 3-D distribution of tropospheric aerosols as characterized by CALIOP, *Atmos. Chem. Phys.*, 13, 3345–3361, doi:10.5194/acp-13-3345-2013, 2013.



- Wood, R.: Stratocumulus Clouds, *Mon. Weather Rev.*, 140, 2373–2423, doi:10.1175/MWR-D-11-00121.1, 2012.
- Wyant, M. C., Bretherton, C. S., Wood, R., Carmichael, G. R., Clarke, A., Fast, J., George, R., Gustafson Jr., W. I., Hannay, C., Lauer, A., Lin, Y., Morcrette, J.-J., Mulcahy, J., Saide, P. E., Spak, S. N., and Ya, Q.: Global and regional modeling of clouds and aerosols in the marine boundary layer during VOCALS: the VOCA intercomparison, *Atmos. Chem. Phys.*, 15, 153–172, doi:10.5194/acp-15-153-2015, 5 2015.
- Yukimoto, S., Adachi, Y., Hosaka, M., Sakami, T., Yoshimura, H., Hirabara, M., Tanaka, T. Y., Shindo, E., TSUJINO, H., DEUSHI, M., MIZUTA, R., YABU, S., OBATA, A., NAKANO, H., KOSHIRO, T., OSE, T., and KITOH, A.: A New Global Climate Model of the Meteorological Research Institute: MRI-CGCM3 -Model Description and Basic Performance-, *J. Meteorol. Soc. Japan. Ser. II*, 90A, 23–64, doi:10.2151/jmsj.2012-A02, 2012.
- 10 Zelinka, M. D., Andrews, T., Forster, P. M., and Taylor, K. E.: Quantifying components of aerosol-cloud-radiation interactions in climate models, *J. Geophys. Res. Atmos.*, 119, 7599–7615, doi:10.1002/2014JD021710, 2014.

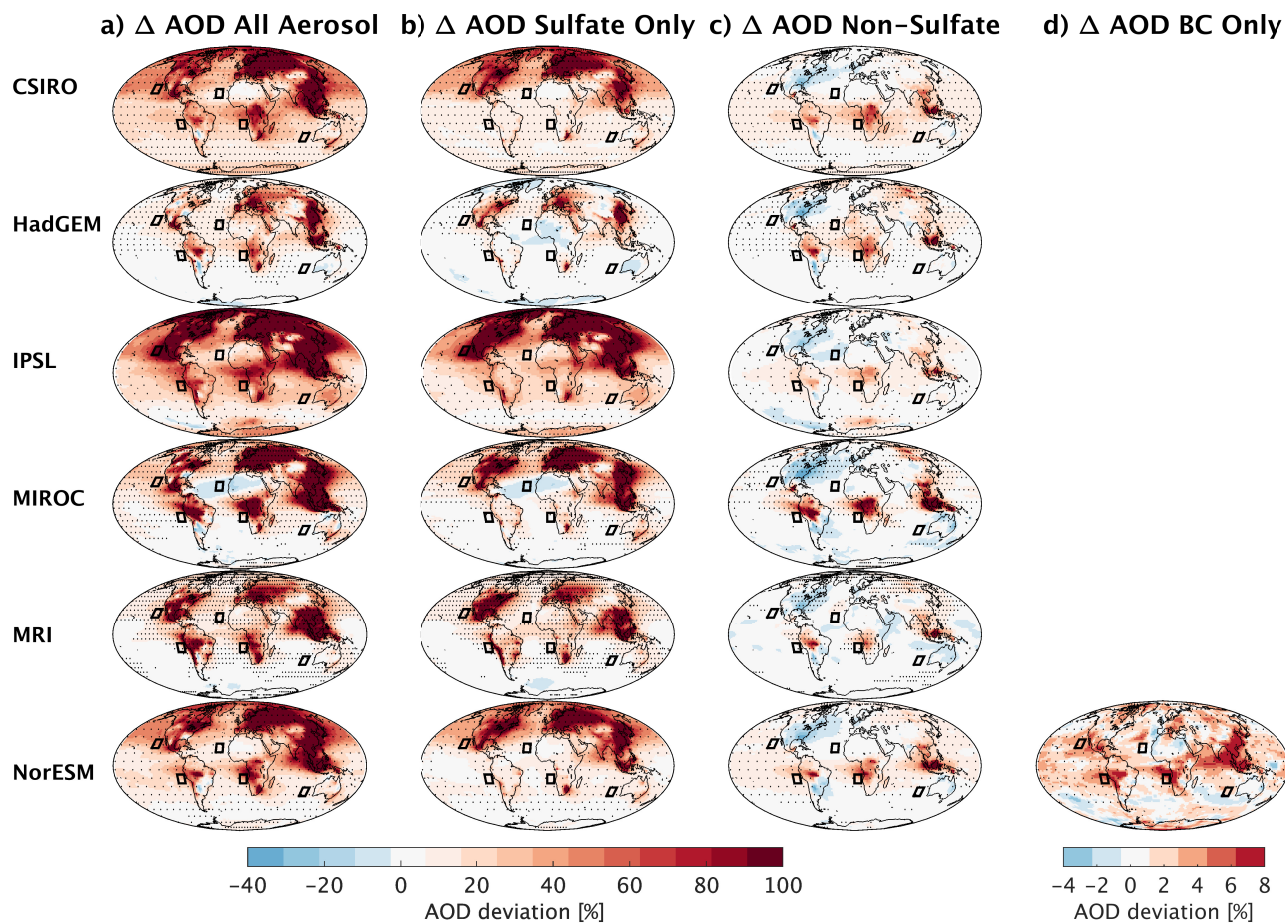


Figure 1. Relative AOD deviation in % between a) the All Aerosol and Control experiment, b) the Sulfate Only and Control experiment, c) the All Aerosol and Sulfate Only experiment for six CMIP5 models, and d) the BC Only and Control experiment for one model. Statistical significance at the 95% level, determined with a t-test, is indicated with stippling, interpolated to a coarser grid. Black boxes indicate the five analysis regions of marine stratocumulus clouds.

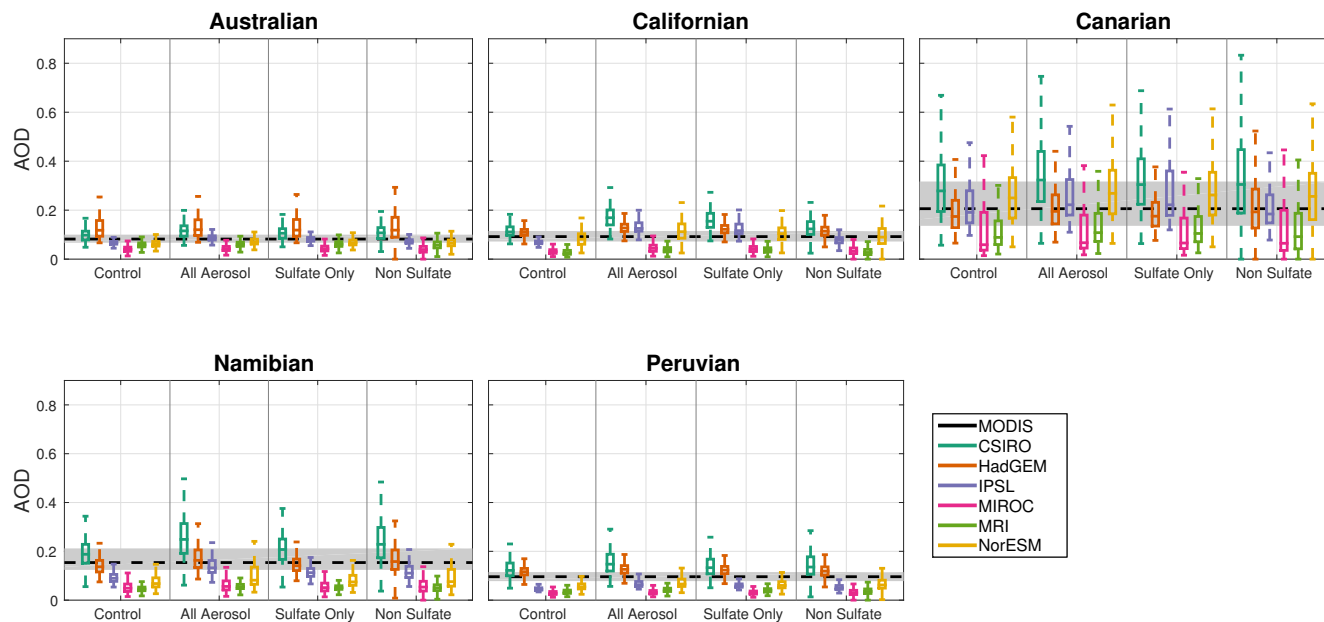


Figure 2. Box-and-whisker plots of total AOD for six CMIP5 models for the Control, All Aerosol, Sulfate Only and Non-Sulfate cases in the Australian, Californian, Canarian, Namibian and Peruvian regions. Median, 25th and 75th percentiles and maximum and minimum AOD are indicated. The data are not de-seasonalized and not de-regionalized. The black dashed line indicates the median AOD value for MODIS satellite observations from 2002 to 2015, and grey shading shows the range between the 25th and 75th percentiles.

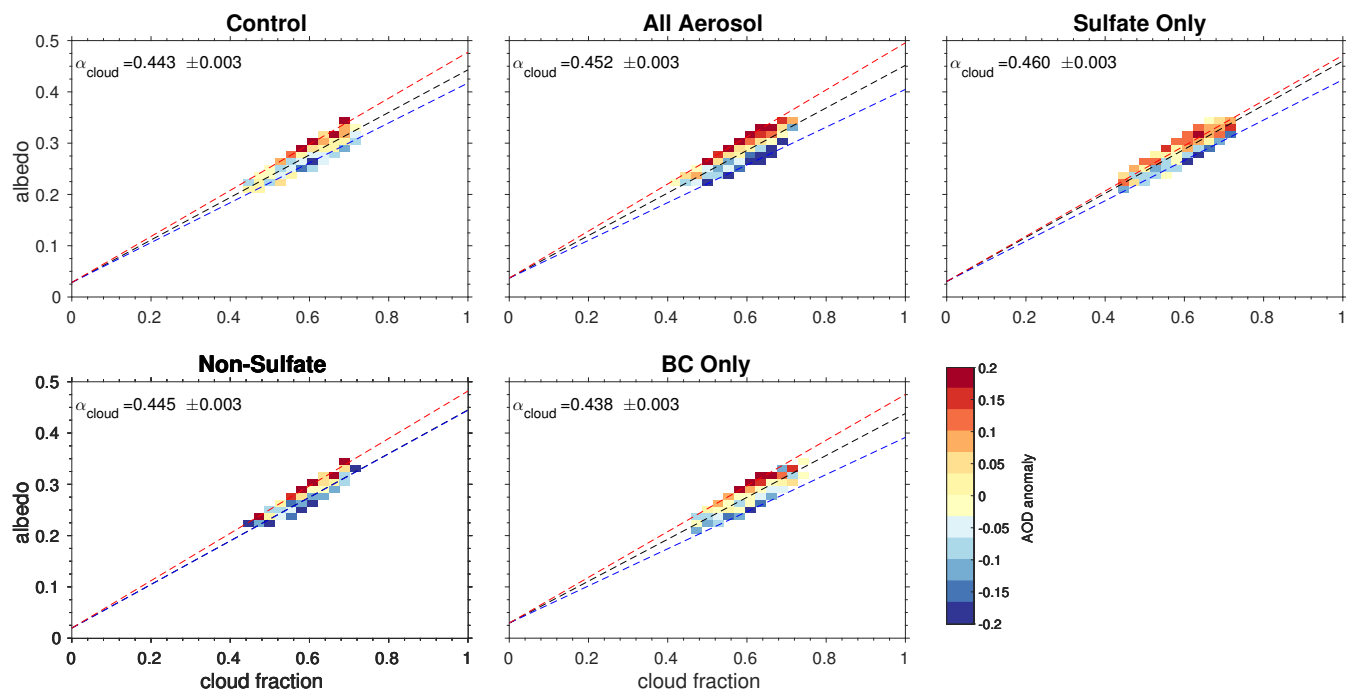


Figure 3. AOD anomaly gradient for the model NorESM for all experiments, in the Californian region. Two linear regressions are performed for the separated upper (red dashed line) and lower (blue dashed line) 10% of the data. The black dashed line represents a linear fit for all the AOD anomaly data, and the estimated cloud albedo is derived from the slope and intercept of that linear regression. The color scale for the anomaly was normalized by the standard deviation of AOD for each cloud fraction bin.

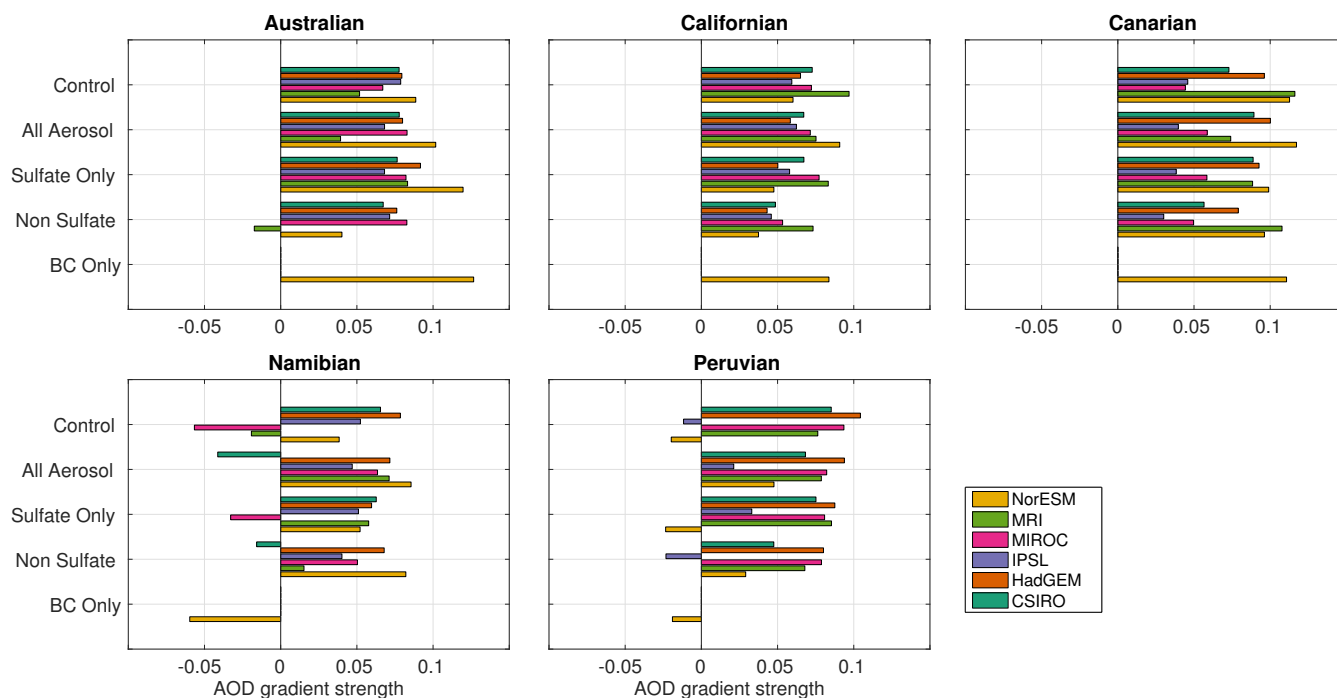


Figure 4. AOD gradient strength quantified by the difference of separate linear regressions for the lower and upper 10th percentile of AOD anomaly points respectively. Values are given for all six CMIP5 models for the Australian, Californian, Canarian, Namibian and Peruvian regions and the Control, All Aerosol, Sulfate Only, Non Sulfate and BC Only (for NorESM) cases.

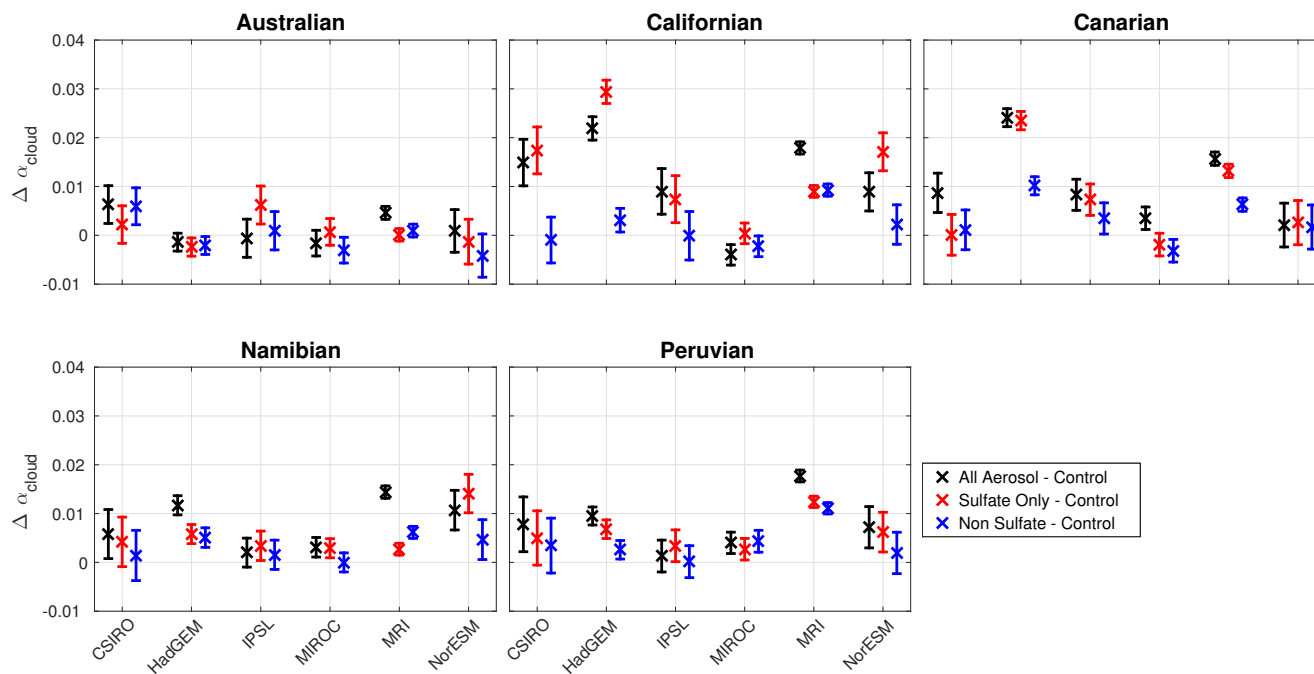


Figure 5. Estimated cloud albedo changes in six CMIP5 models for the Australian, Californian, Canarian, Namibian and Peruvian regions, due to changes in emissions of all anthropogenic aerosols (black), sulfate only (red) and non-sulfate (blue). Errorbars indicate one standard deviation.

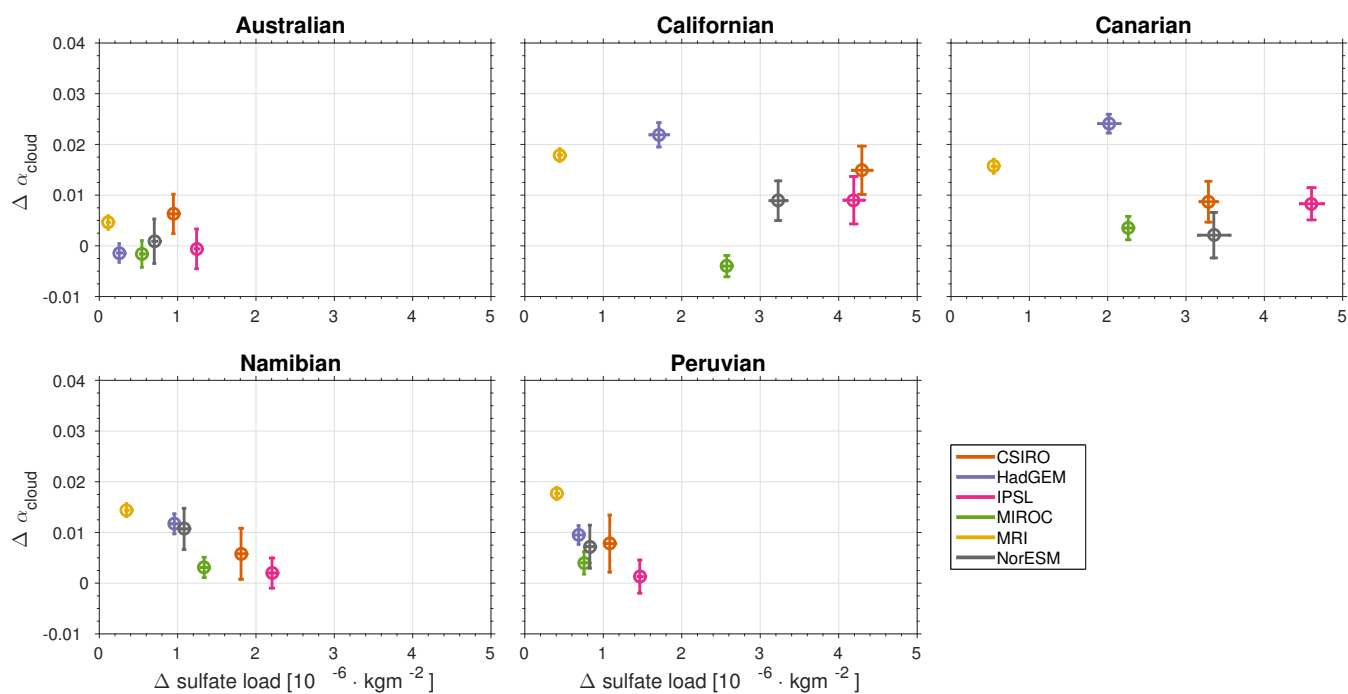


Figure 6. Scatter plot of change in cloud albedo and change in sulfate load due to all anthropogenic aerosols, for six CMIP5 models for the Australian, Californian, Canarian, Namibian and Peruvian regions. Errorbars indicate one standard deviation.

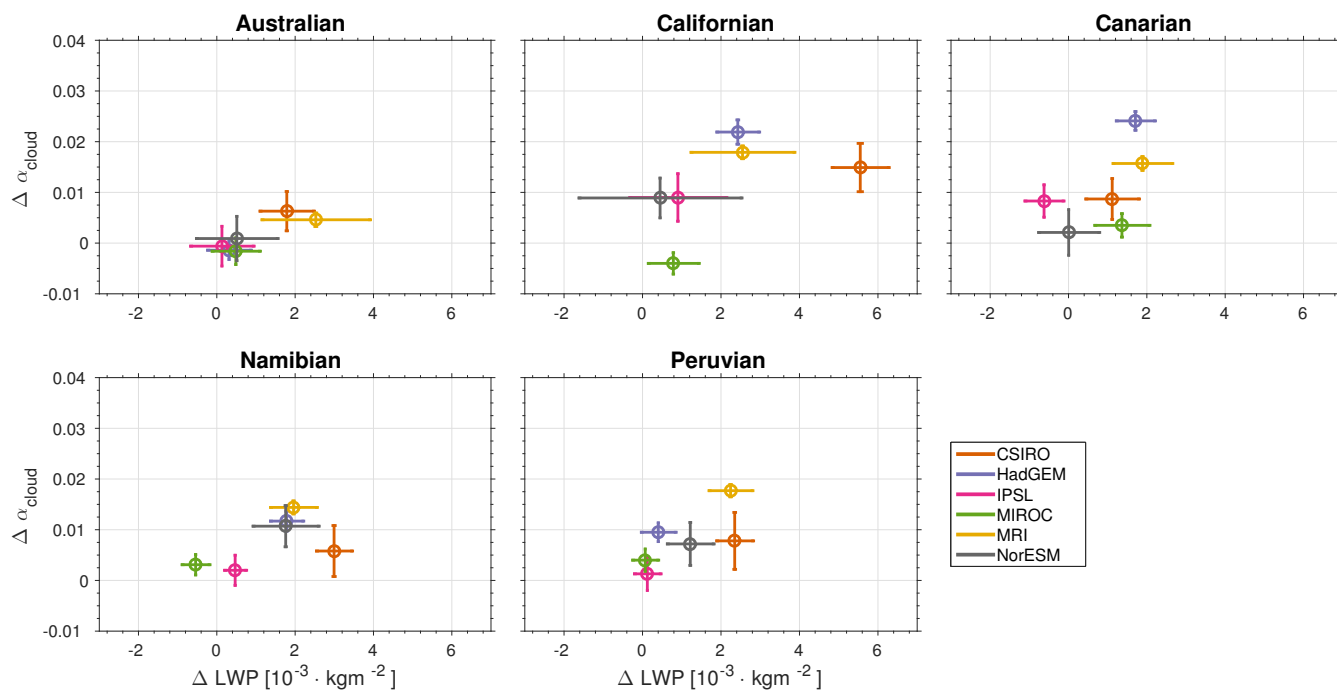


Figure 7. Scatter plot of change in cloud albedo and change in LWP due to all anthropogenic aerosols, for six CMIP5 models for the Australian, Californian, Canarian, Namibian and Peruvian regions. Errorbars indicate one standard deviation.

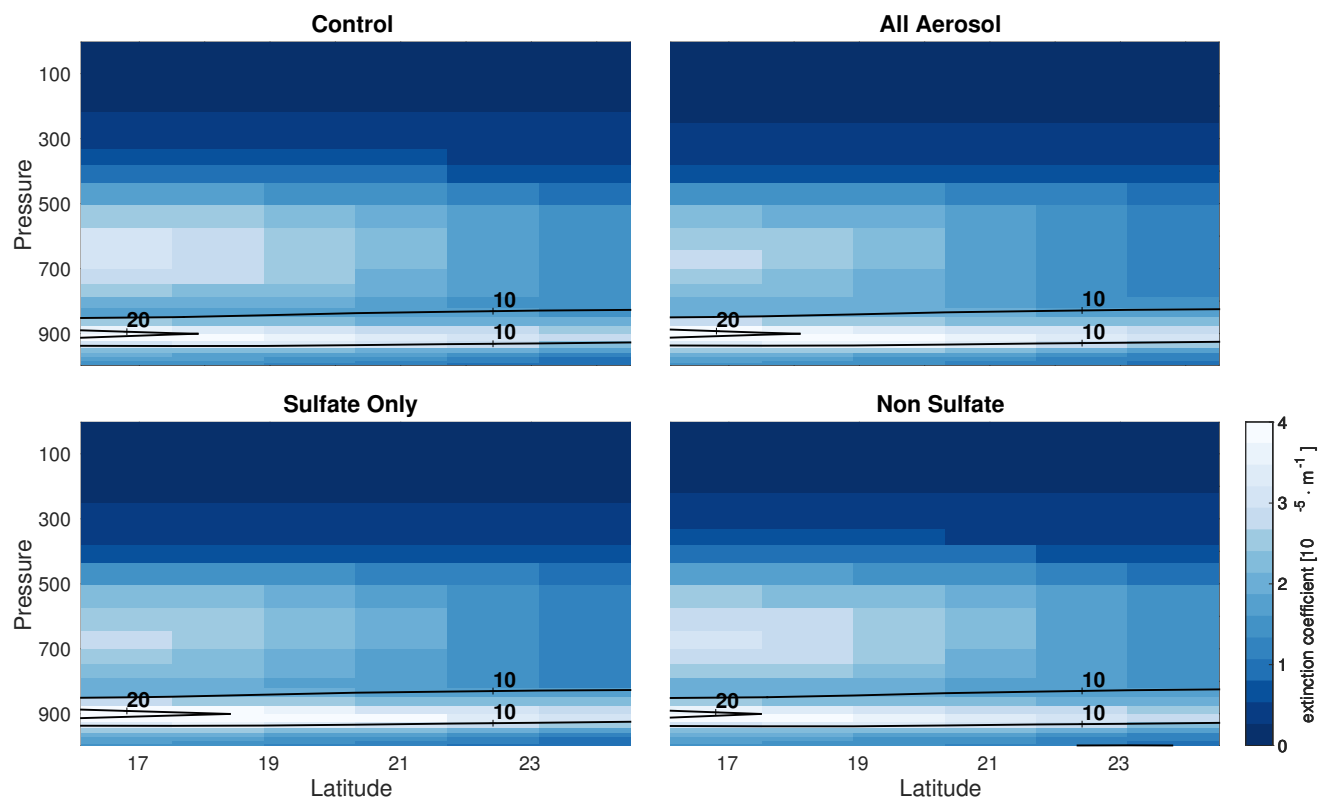


Figure 8. Vertical distribution of the aerosol extinction coefficient at 550 nm (colour) and the cloud fraction in % (contours) for the model MIROC in the Canarian region.

**Table 1.** Models considered in the study, where the short names listed are used through.

Model	Short name	Institute	Resolution	Cloud albedo/ lifetime effect	Reference
CSIRO-Mk3-6-0	CSIRO	CSIRO-QCCCE	T63 L18	yes/ yes	Rotstayn et al. (2012)
HadGEM2-A	HadGEM	MOHC	N96 L38	yes/ yes	Bellouin et al. (2007); Collins et al. (2011)
IPSL-CM5A-LR	IPSL	IPSL	96 x 95 x 39	yes/ no	Dufresne et al. (2013)
MIROC5	MIROC	MIROC	T85 L40	yes/ yes	Takemura et al. (2005); Watanabe et al. (2011)
MRI-CGCM3	MRI	MRI	TL159 L48	yes/ yes	Yukimoto et al. (2012)
NorESM1-M	NorESM	NCC	f19 L26	yes/ yes	Iversen et al. (2013); Kirkevåg et al. (2013)



Table 2. Relative contributions to the total loading in % for the Control experiment. OM for NorESM includes only primary organic aerosol and for HadGEM only secondary organic aerosol.

Region	Model	Relative loading contributions				
		sulfate	BC	OM	dust	sea salt
Australian	CSIRO	6	< 1	11	28	54
	HadGEM	1	< 1	1	34	64
	IPSL	2	< 1	2	7	89
	MIROC	4	< 1	3	43	50
	MRI	1	< 1	1	5	93
	NorESM	5	< 1	16	11	67
Californian	CSIRO	6	< 1	10	42	41
	HadGEM	1	< 1	2	27	70
	IPSL	4	< 1	6	29	60
	MIROC	3	< 1	4	67	26
	MRI	2	< 1	1	10	87
	NorESM	6	1	20	39	35
Canarian	CSIRO	1	< 1	1	93	5
	HadGEM	1	< 1	1	68	30
	IPSL	1	< 1	1	87	12
	MIROC	1	< 1	1	92	6
	MRI	< 1	< 1	< 1	78	21
	NorESM	2	< 1	3	87	8
Namibian	CSIRO	2	< 1	7	78	13
	HadGEM	1	< 1	4	41	54
	IPSL	2	< 1	6	62	29
	MIROC	3	< 1	8	57	32
	MRI	2	1	5	13	79
	NorESM	5	1	31	21	41
Peruvian	CSIRO	4	< 1	7	66	23
	HadGEM	2	< 1	4	20	74
	IPSL	5	< 1	7	8	80
	MIROC	8	< 1	7	27	59
	MRI	3	< 1	2	2	93
	NorESM	10	< 1	31	10	49



Table 3. Temporal and spatial correlation coefficients between individual aerosol loadings and the total AOD for all models and regions for the Control experiment. OM for NorESM includes only primary organic aerosol and for HadGEM only secondary organic aerosol. All correlations are significant at the 95% level.

Region	Model	Correlation coefficient				
		sulfate	BC	OM	dust	sea salt
Australian	CSIRO	0.39	0.65	0.64	0.69	0.15
	HadGEM	0.53	-0.19	-0.10	0.89	0.18
	IPSL	-0.41	0.18	-0.06	0.27	0.96
	MIROC	0.20	0.32	0.31	0.43	0.79
	MRI	-0.19	0.09	0.08	0.27	0.82
	NorESM	0.03	0.16	0.29	0.44	0.74
Californian	CSIRO	0.86	0.83	0.84	0.58	-0.28
	HadGEM	0.63	0.15	0.50	0.60	-0.08
	IPSL	0.81	0.71	0.80	0.73	-0.42
	MIROC	0.48	0.35	0.36	0.66	0.26
	MRI	0.13	-0.01	-0.21	0.49	0.84
	NorESM	0.59	0.76	0.69	0.68	-0.23
Canarian	CSIRO	-0.07	0.08	0.38	0.98	-0.17
	HadGEM	0.29	0.02	0.03	0.97	0.36
	IPSL	0.80	-0.3	0.27	0.99	-0.52
	MIROC	0.17	-0.18	0.02	1.00	0.41
	MRI	-0.25	0.30	0.13	0.99	0.55
	NorESM	0.58	0.30	0.38	0.94	-0.26
Namibian	CSIRO	0.46	0.69	0.79	0.83	-0.36
	HadGEM	0.34	0.27	0.27	0.91	-0.38
	IPSL	0.69	0.35	0.43	0.82	-0.44
	MIROC	0.64	0.69	0.68	0.83	0.47
	MRI	0.20	0.36	0.32	0.36	0.65
	NorESM	0.72	0.93	0.92	0.39	0.40
Peruvian	CSIRO	0.38	0.59	0.79	0.78	-0.29
	HadGEM	0.67	0.24	0.59	0.37	-0.16
	IPSL	0.20	0.73	0.88	0.64	0.04
	MIROC	-0.03	0.73	0.75	0.24	0.59
	MRI	0.14	-0.07	-0.14	-0.03	0.89
	NorESM	0.43	0.75	0.90	0.48	0.13